Journal of Solid State Chemistry 184 (2011) 2655–2660

Contents lists available at ScienceDirect

Journal of Solid State Chemistry

journal homepage: www.elsevier.com/locate/jssc

Preparation and characterization of ordered porous carbons for increasing hydrogen storage behaviors

Seul-Yi Lee, Soo-Jin Park*

Department of Chemistry, Inha University, 253 Nam-gu, Incheon 402-751, South Korea

ARTICLE INFO

Article history:
Received 6 May 2011
Received in revised form
13 July 2011
Accepted 18 July 2011
Available online 26 July 2011

Keywords:
Hydrogen storage
Ordered porous carbons
FT-Raman spectroscopy
Transmission Electron Microscopy
Carbonization temperature

ABSTRACT

We prepared ordered porous carbons (PCs) by using a replication method that had well-organized mesoporous silica as a template with various carbonization temperatures in order to investigate the possibility of energy storage materials. The microstructure and morphologies of the samples are characterized by XRD, TEM, and FT-Raman spectroscopy. N_2 adsorption isotherms are analyzed by the *t*-plot method, as well as the BET and the H–K method in order to characterize the specific surface area, pore volume, and pore size distribution of the samples, respectively. The capacity of the hydrogen adsorption of the samples is evaluated by BEL-HP at 77 K and 1 bar. From the results, we are able to confirm that the synthesis of the samples can be accurately governed by the carbonization temperature, which is one of the effective parameters for developing the textural properties of the carbon materials, which affects the behaviors of the hydrogen storage.

1. Introduction

Hydrogen is currently being considered as an ideal energy source that would replace fossil fuels. There are still a few technological and scientific issues that require improvement, in particular, how it will be stored in a safe and efficient way, which is the key in developing reliable hydrogen technology. Currently, many methods for storing hydrogen have involved cryogenic liquefied hydrogen, which is chemical hydrogen storage in an atomic form, as well as metal hydrides composed of complex hydrides, compressed hydrogen, and physisorption of hydrogen on porous materials [1–5]. Cryogenic liquid hydrogen and chemical hydrogen storage methods have the highest cost while their technologies have low energy efficiency. Compressed hydrogen has necessitated the building of storage devices for the advanced composite material due to its very high pressures. Meanwhile, the physisorption of gaseous hydrogen is a good choice because of its high energy efficiency and weak bonding in gas–solid interactions [6–9].

Carbon-based materials, such as activated carbons, carbon nanotubes, and carbon fibers have received much attention as candidates of the physisorption of hydrogen due to their being lightweight, having abundant natural precursors, and costing less [10–13]. However, carbon nanotubes or carbon fibers have a relatively low specific surface area compared to other porous carbon materials while activated carbons have generally poorly controlled distributions of pore size and the presence of metal impurities in the precursor. More than half of the total pore volumes come from macropores in spite of a very high specific surface area, which hinders their application as hydrogen storage materials [14]. Recently, porous carbons have been characterized as being well-organized structure with high specific surface area, but a narrow micropore size distribution is being considered as a more eligible candidate for hydrogen physisorption [15,16].

Porous carbons can be synthesized by many methods [16–22] with the templating method being one of the most commonly used techniques. This method consists of the infiltration of an inorganic template (*e.g.*, MCM-41, MCM-48, SBA-15, KIT-6, and so on) with an appropriate carbon precursor (*e.g.*, sucrose, furfuryl alcohol [22], phenol resin [23], mesophase pitch [24], and polyvinylbenzene [25]), followed by the carbonization of the precursor and subsequent removal of the inorganic templates with an HF or NaOH solution in order to create a porous carbon network. This porous carbon network may provide a high specific surface area, large pore volume, and in particular, precise pore structure control through replicating the structure of the inorganic templates. Also, the ordered networks of porous carbons may provide fast transportation through the materials. A noticeable volume of micropores can efficiently adsorb hydrogen, while the micro- and meso-porosity can be adjusted by changing the template.

The aim of this work is to examine the effect of the carbonization temperature on the structure and texture, as well as hydrogen storage behaviors, of ordered porous carbons. The porous carbons were synthesized with a sucrose solution as carbon sources using the well-organized silicas SBA-15 as a template.

* Corresponding author. Fax: +82 32 860 8438.
E-mail address: sjpark@inha.ac.kr (S.-J. Park).

0022-4596/$ - see front matter © 2011 Elsevier Inc. All rights reserved.
doi:10.1016/j.jssc.2011.07.034

The hydrogen storage capacity was influenced by the textural properties of the porous carbons samples, resulting in the development of microporosity and graphitization.

2. Experimental section

2.1. Materials and sample preparation

The ordered porous carbons (PCs) were prepared by a well-known templating procedure [26–30] for which the mesoporous silica SBA-15 was chosen as the silica template and sucrose was chosen as the carbon precursor. The parent SBA-15 silica was synthesized by using the procedures specified in [31–33] where a non-ionic oligomeric alkyl-ethylene oxide surfactant was used as the structure directing agent that became known as, Pluronic P123. The 1.0 g of synthesized SBA-15 was impregnated with an aqueous solution of 1.25 g sucrose, 0.14 g sulfuric acid, and 5.0 g distilled water. The mixture was stirred for 1 h, followed by aging at 100 °C for 6 h, then at 160 °C for 6 h. The aged mixture was grounded into powder and added to a solution of 0.8 g sucrose, 0.09 g sulfuric acid, and 5.0 g distilled water, which was stirred for 1 h, followed by further aging, which was similar to what was described above. About 1.0 g of the resulting powder was placed in the furnace, which was set to a heating rate of 5 °C min^{-1} under an N_2 gas flow, in order to reach the target carbonization temperature. There, the temperature was maintained for 5 h. With all samples, SBA-15 silica template was removed by leaching it with a 5% by weight HF aqueous solution. The samples were then washed with distilled water several times thoroughly and dried in a vacuum oven for 24 h at 120 °C. The prepared PCs with various carbonization temperatures ranging from 650 to 1100 °C were named T-650, T-800, T-950, and T-1100.

2.2. Characterization methods

X-Ray diffraction (XRD) patterns were obtained using a Rigaku Model D/MAX diffractometer with CuKα radiation operating at 40 kV and 40 mA. The patterns were recorded with a scan step time of 2 s and a step size of 0.02°. Transmission Electron Microscope (TEM) images were recorded on a JEOL Co., Model JEM 2100 F electron microscope operating at 200 kV. FT-Raman analyses were employed by using a Bruker Model RFS 100/S with the excitation wavelength of a He–Ne laser being 600 nm while the power was 500 mV. The porous textural characterization of all the samples was measured at 77 K by using a gas adsorption analyzer, BEL Co., Ltd.'s Model BEL-SORP. The samples were degassed at 573 K for 6 h in order to obtain a residual pressure that was less than 10^{-6} mmHg. Specific surface areas and the micropore volume of the samples were determined from the Brunauer–Emmett–Teller (BET) equation and the *t*-plot method, respectively. The amounts of N_2 adsorbed at relative pressures (P/P_0=0.98) were used to investigate the total pore volumes, which corresponded to the sum of the micropore and mesopore volume.

2.3. Hydrogen storage capacities

The hydrogen uptake experiment was conducted under 77 K and 1 bar. In each experiment, about 0.5 g of sample was loaded into a stainless chamber. Prior to the measurement, the system was evacuated for 12 h while the sample chamber was heated to 473 K. After the chamber was cooled to room temperature, hydrogen was introduced with pressure. An ultra-high-purity grade (99.9999%) of hydrogen was used, so that the influences of moisture and other impurities could be excluded. Finally, we used a volumetric measurement method to determine the hydrogen uptake capacity.

3. Results and discussion

3.1. Characterization

Fig. 1 shows the XRD patterns of the SBA-15 and of the PCs samples with various carbonization temperatures. Except for the T-650 sample, all samples exhibit intense peaks in the 2 theta of 0.9–1.0° due to (1 0 0) reflection and small peaks due to higher order (1 1 0) and (2 0 0) reflections, which indicates the formation of porous materials with hexagonal arrays [33,34]. It should be revealed that their primary structure of hexagonally arranged carbon nanorods was retained. Meanwhile, the noticeable broadening of the (1 0 0) peak intensity in the T-1100 sample may be attributed to a partial collapse of the long-range order because of poor hydrothermal stability and a little disorder of the structure due to the excessive carbonization temperature. In addition, when the carbonization temperature was performed up to 650 °C, no resolved XRD peak at low angles was observed. This meant it was not well-organized in this carbonization process of 650 °C, indicating the lack of an ordered pore arrangement. It might be attributable to the poor graphitization. This will be further shown in good agreement with the value determined from FT-Raman analysis. At the same time, the position of the interplanar spacing of (1 0 0) reflection, d_{100} for the PCs samples, was shifted towards

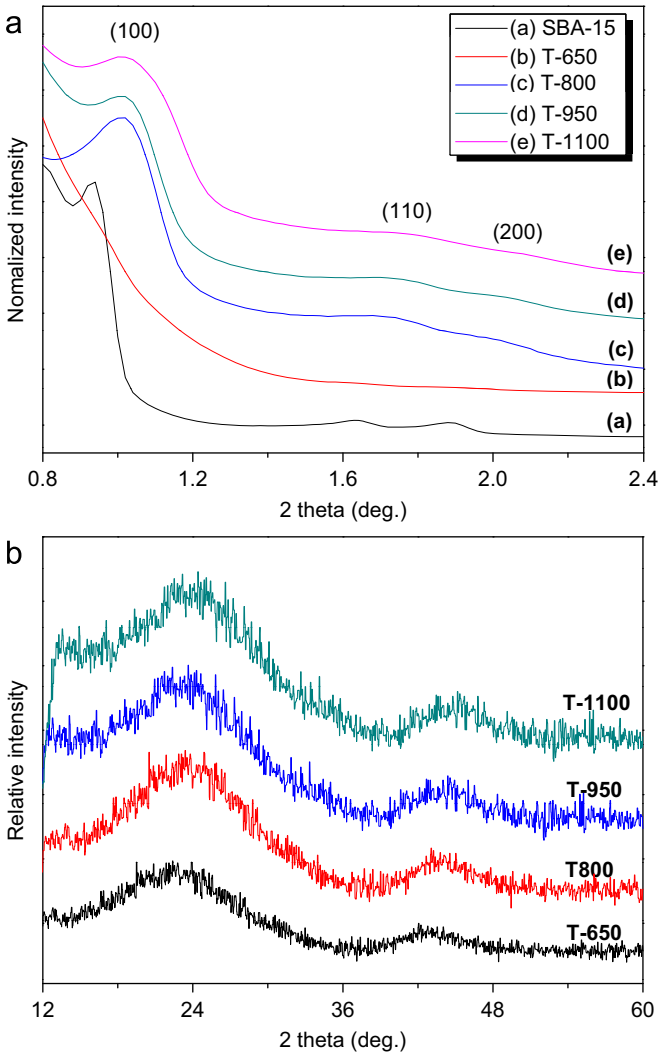

Fig. 1. Low-angle (a) and high-angle (b) XRD patterns of the SBA-15 and the PCs with various carbonization temperatures.

higher angles, which indicated a decrease in the lattice parameter. The d_{100} and the hexagonal lattice parameter a_0 of the SBA-15 and the PCs samples are listed in Table 1. It is shown that both parameters of the PCs samples decreased with an increase in the carbonization temperature, which might be due to the formation of a smaller structure. This appearance can be attributed to the structural shrinkage of the silica framework that occurred during the carbonization process [35,36]. It is found that the pore wall thickness of PC samples decreases with increasing the carbonization temperatures. As for the reflections at a higher angle, the diffraction peak around 2 theta=23° corresponded to the (0 0 2) reflection planes (interlayered spacings between adjacent graphite layers) slightly shifted upward with an increase in the carbonization temperature. It was found that the higher carbonization temperature may have improved the degree of graphitization. The average *d*-spacing values of the PCs samples were calculated by using Bragg's law in the range of 3.386–3.410 Å, which was slightly higher with respect to graphite (3.3 Å).

The TEM morphologies of the SBA-15 and T-950 sample are presented in Fig. 2. It is well illustrated that the somewhat considerable long-range ordering and the presence of mono-dimensional aligned channels between the two aligned nanorods of the porous framework was retained in the T-950 sample during the carbonization process. It was also confirmed that the pore structures in the T-950 sample shrunk in comparison to the SBA-15 sample.

The FT-Raman spectra of the PCs samples with various carbonization temperatures are shown in Fig. 3, which is a very valuable tool for characterizing the graphite carbon materials [37]. A single graphitic crystal exhibited only one vibrational mode above 1000 cm^{-1}, namely the G-band located around 1600 cm^{-1} which corresponded to the tangential C–C stretching vibration. In small crystallites of graphitic carbon or amorphous carbon materials, additional bands detected the D-band being located around 1300 cm^{-1} due to the local defects that originated from structural imperfections. With all the PCs samples, two characteristic bands were seen due to the G- and D-band. It was found that the relative intensities significantly increased with an increase in the carbonization temperature, indicating that a higher degree of graphitization can be obtained at higher temperatures. Also, with an increase in the carbonization temperature, the G- and D-band slightly shifted to higher and lower wavenumbers, respectively. This might be due to an increased orientation and domain of nano-graphene layers, as well as the stacking of parallel graphene layers. These results were in good accordance with high-angle XRD patterns.

The obtained N_2/77 K adsorption/desorption isotherms of the SBA-15 and the PCs samples with various carbonization temperatures are displayed in Fig. 4. As shown in Fig. 4, at a relative pressure below 0.1, all the samples had steadily increasing amounts of adsorption, indicating the largest amounts of micropores. Along with an increase in relative pressure, steady increases in adsorption capacity were caused by the monolayer/multilayer adsorptions of nitrogen molecules on the mesopores or macropores. Also, the hysteresis of the PCs samples was observed in a relative pressure range of 0.4–0.6, which was attributed to the capillary condensation of nitrogen molecules in mesopores

Table 1
XRD parameters of the SBA-15 and the PCs samples with various carbonization temperatures.

Specimens	*d*-Spacing (nm)[a]	a_0 (nm)[b]	*W* (nm)[c]
SBA-15	9.4	10.9	5.0
T-650	–	–	–
T-800	8.7	10.1	5.5
T-950	8.6	10.0	5.3
T-1100	8.5	9.8	5.0

[a] Periodicity of the SBA-15 and the PCs samples with various carbonization temperature, determined from Bragg reflection of (1 0 0).
[b] Lattice parameter of the SBA-15 and the PCs samples with various carbonization temperature, calculated as $a_0=2d_{100}/\sqrt{3}$.
[c] Pore wall thickness was calculated as $W=a_0-D$.

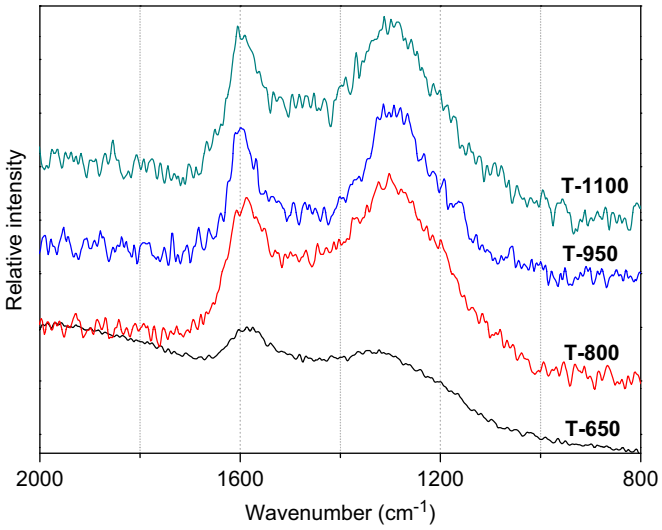

Fig. 3. FT-Raman spectra of the SBA-15 and the PCs with various carbonization temperatures.

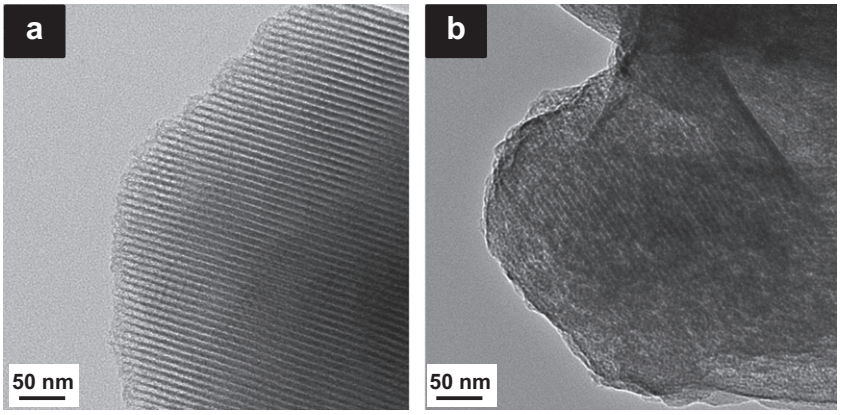

Fig. 2. TEM images of the SBA-15 (a) and the T-950 sample (b).

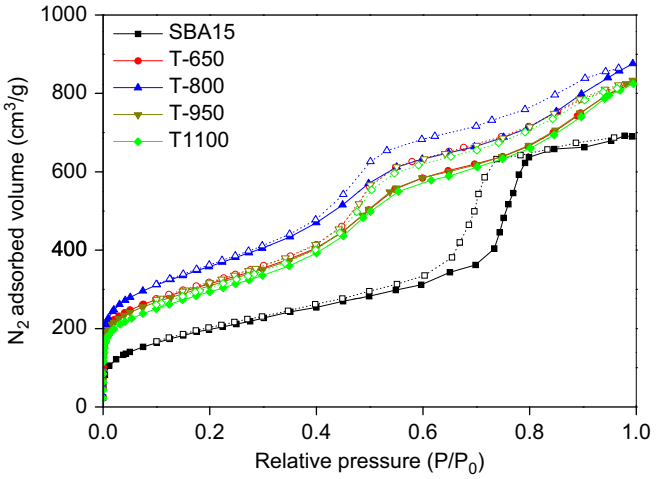

Fig. 4. N_2/77 K adsorption/desorption isotherms of the SBA-15 and the PCs with various carbonization temperatures.

with relatively uniform dimensions that were in 2-D hexagonally ordered cylindrical channels [38,39].

As shown in Fig. 5, we can find that the pore structures of the SBA-15 in the PCs samples remained well intact during the carbonization process, which led to more uniform pore size distributions. It also became very interesting that the specific surface area and total pore volume of the PCs samples remarkably increased in comparison to SBA-15. In order to understand the pore structures of the samples in detail, Table 2 lists the textural properties of the SBA-15 and the PCs samples with various carbonization temperatures. Table 2 clearly shows that the specific surface area and total pore volume increased when the carbonization temperature of 800 °C was applied, which may be attributable to the fact that a higher carbonization temperature is helpful in forming well-organized porous carbon structures. Meanwhile, the carbonization process with an excessively high temperature induced a decrease in the textural properties of the PCs samples due to the lattice contraction of the silica framework from heating treatments, as shown in the T-950 and T-1100 samples. According to the results, it was found that the T-800 sample had the highest specific surface area while the total pore volume values were 1270 $m^2\ g^{-1}$ and 1.350 $cm^3\ g^{-1}$. It was also observed that the micropore volume was decreased from T-800 to T-1100, which is corresponded with decreasing of the pore wall thickness (as previously shown in Table 1). It was interesting to note that the thicker pore wall has more defects (micropores) in contains, resulting from the increasing amount of stress-induced defects in the thicker wall [40].

Fig. 5 shows the micro-(a) and meso-(b) pore size distributions of the SBA-15 and the PCs samples with various carbonization temperatures, which were determined by the Horvath–Kawazoe (H–K) and Barrett–Joyner–Halenda (BJH) methods, respectively. The micropore size distributions showed a distribution of micropores ranging between 0.4 and 0.8 nm. It can be seen that the micropores ranged from 0.6 to 0.7 nm, which has been previously reported to be the optimum pore size for hydrogen storage [41–44]. The size of the centered peaks of the micropores in the PCs samples shifted to the left side with an increase in the carbonization temperature due to the shrinkage of the silica framework from heating treatments, as previously mentioned. Moreover, it was found that the mesopore size was reduced from about 8.1 nm for the SBA-15 to about 3.7 nm for the PCs samples. This feature was in accordance with the XRD patterns, *i.e.*, the structural shrinkage of the silica framework that occurred during the carbonization process.

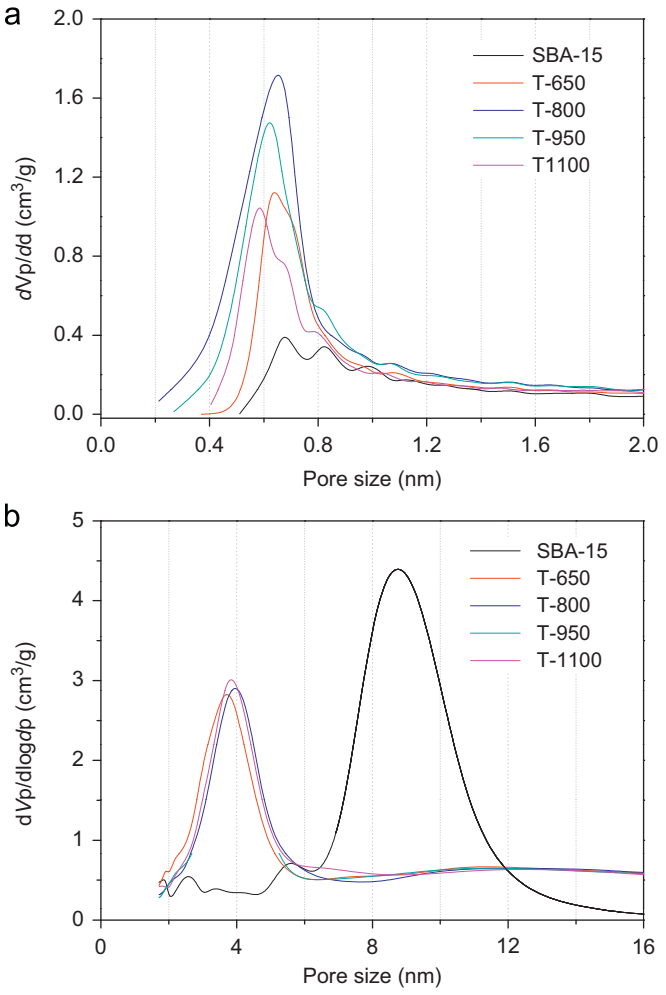

Fig. 5. Micro-(a) and meso-(b) pore size distributions of the SBA-15 and the PCs with various carbonization temperatures.

Table 2
N_2/77 K textural properties of the SBA-15 and the PCs samples with various carbonization temperatures.

Specimens	S_{BET} (m^2/g)[a]	V_{Total} (cm^3/g)[b]	V_{Micro} (cm^3/g)[c]	D (nm)[d]
SBA-15	725	1.068	0.187	5.88
T-650	1110	1.277	0.592	4.60
T-800	1270	1.350	0.627	4.25
T-950	1090	1.294	0.520	4.68
T-1100	1005	1.270	0.502	4.83

[a] S_{BET}: specific surface area computed using BET equation in a relative pressure range of 0.2–0.3.
[b] V_{Total}: total pore volume is estimated at a relative pressure P/P_0=0.99.
[c] V_{Micro}: micropore volume is calculated from *t*-plot method.
[d] D: adsorption average pore width determined from BET method.

3.2. Hydrogen uptake capacities

Fig. 6 shows the hydrogen storage capacity values of the SBA-15 and the PCs samples with various carbonization temperatures at 77 K and sub-atmospheric pressure. As to the hydrogen storage at 77 K, the physisorption mechanism was dominant while hydrogen adsorption behaviors were driven by the textural properties of adsorbent materials. In particular, for the carbon nano-materials, hydrogen adsorption depended strongly on the micropores. The results of this study correspond with those of an earlier report [45–47]. From the results, it seems that the actual

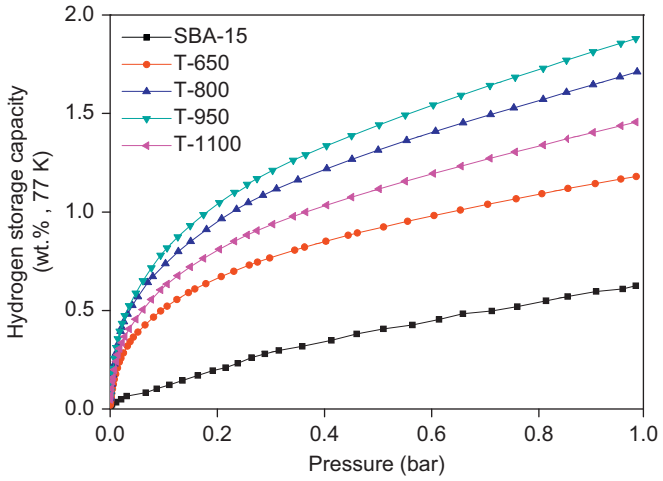

Fig. 6. Hydrogen storage capacity of the SBA-15 and the PCs with various carbonization temperatures.

order of the hydrogen storage capacity was roughly similar to that of the micropore volume. It was expected that the PCs samples with a higher micropore volume would have more accessible adsorbing sites, resulting in adsorption capacity. However, it was interesting to note that the T-950 sample had the highest hydrogen storage capacity, although the micropore volume of the T-950 sample was lower than the T-800 sample. As shown in Fig. 5, this result was attributed to the micropore size distribution where the T-950 sample was further shifted to the left side in comparison to the T-800 sample. It was indicated that the pore size of the T-950 sample became smaller due to the higher carbonization temperature, resulting in an enhancement in the hydrogen storage capacity of the T-950 sample. Therefore, the carbonization temperature probably played an important role in shrinking the micropores during the carbonization process of the PCs.

In addition, it was found that the hydrogen storage capacity of the T-650 sample had remarkably low values, with 1.2 wt%, in spite of the fact that the T-650 sample had a considerably high specific surface area and micropore volume. It has been suggested that the degree of graphitization on the PCs samples played a significant role in the PCs' surfaces characteristics, which had an attractive force on hydrogen molecules, which resulted in improving the hydrogen storage capacity.

From the results, it can be seen that an optimum condition for the higher hydrogen storage capacities of the PCs samples existed after being treated with a carbonization process at 950 °C, where the hydrogen storage capacity of 1.9 wt% was obtained at 77 K and 1 bar. In this work, the degree of graphitization led to an increase in hydrogen storage capacity in the presence of well-developed micropore volume or size distribution [48–50].

4. Conclusions

In this work, we prepared ordered porous carbons (PCs) by using the replication method SBA-15 as a template. We also observed the effect of carbonization temperature on the carbonization process, especially related to the textural and structural characteristics of the PCs, in order to investigate the possibility of energy storage materials. From the results, it was found that the enhancement in the hydrogen storage capacity was associated with the textural properties (*i.e.*, specific surface area and pore volume) and micropore size distribution, as well as structural properties, which were optimum conditions caused by the carbonization temperature at 950 °C. In particular, a considerable increase in the hydrogen storage capacity of the T-950 sample was due to the strongly suitable pore size of the PCs materials for hydrogen adsorption. Conseqeuntly, the volume and size distribution of the micropore, as well as the structural properties, were good parameters for enhancing the hydrogen storage capacity of these ordered porous carbon materials. This can lead to important applications in the field of hydrogen storage materials. Furthermore, these micropores might be used as such or after convenient functionalization, oxides dispersion, or metal doping for enhancing the hydrogen storage capacity.

Acknowledgment

This work was supported by the Carbon Valley Project of the Ministry of Knowledge Economy, Korea.

References

[1] L. Schlapbach, A. Züttel, Nature 414 (2001) 353–358.
[2] H. Kajiura, S. Tsutsui, K. Kadono, M. Kakuta, M. Ata, Y. Murakami, Appl. Phys. Lett. 82 (2003) 1105–1107.
[3] B. Sakintuna, F. Lamari-Darkrim, M. Hirscher, Int. J. Hydrogen Energy 32 (2007) 1121–1140.
[4] N.L. Rosi, J. Eckert, M. Eddaoudi, D.T. Vodak, J. Kim, M. O'Keeffe, O.M. Yaghi, Science 300 (2003) 1127–1129.
[5] K. Doi, S. Hino, H. Miyaoka, T. Ichikawa, Y. Kojima, J. Power Sources 196 (2011) 504–507.
[6] H. Takagi, H. Hatori, Y. Soneda, N. Yoshizawa, Y. Yamada, Mater. Sci. Eng. B 108 (2004) 143–147.
[7] S.J. Park, S.Y. Lee, Carbon Lett. 10 (2009) 19–22.
[8] R. Ströbel, J. Garche, P.T. Moseley, L. Jörissen, G. Wolf, J. Power Sources 159 (2006) 781–801.
[9] S.J. Park, S.Y. Lee, J. Colloid Interface Sci. 346 (2010) 194–198.
[10] B.J. Kim, Y.S. Lee, S.J. Park, Int. J. Hydrogen Energy 33 (2008) 2254–2259.
[11] S.Y. Lee, S.J. Park, Bull. Korean Chem. Sci. 31 (2010) 1596–1600.
[12] S.Y. Lee, S.J. Park, J. Solid State Chem. 183 (2010) 2951.
[13] S.J. Park, B.J. Kim, Y.S. Lee, M.J. Cho, J. Int., Hydrogen Energy 33 (2008) 1706–1710.
[14] A. Reyhania, S.Z. Mortazavi, A. Nozad Golikand, A.Z. Moshfegh, S. Mirershadi, J. Power Sources 183 (2008) 539–543.
[15] H. Kabbour, T.F. Baumann, J.H. Satcher, A. Saulnier, C.C. Ahn, Chem. Mater. 18 (2006) 6085–6087.
[16] J. Burress, M.M. Beckner, R. Cepel, G. Suppes, C. Wexler, P. Pfeifer, Nanotechnology 20 (2009) 204026–204036.
[17] G. Abellán, A.I. Carrillo, N. Linares, E. Serrano, J. García-Martínez, J. Solid State Chem. 182 (2009) 2141–2148.
[18] Z. Hu, M.P. Srinivasan, Y. Ni, Adv. Mater. 12 (2000) 62–65.
[19] R. Ryoo, S.H. Joo, K. Kruk, M. Jaroniec, Adv. Mater. 13 (2001) 677–681.
[20] C.M. Yang, C. Weidenthaler, B. Spliethoff, M. Mayanna, F. Schuth, Chem. Mater. 17 (2005) 355–358.
[21] B. Xu, L. Peng, G. Wang, G. Cao, F. Wu, Carbon 48 (2010) 2377–2380.
[22] J.R.C. Salgado, F. Alcaide, G. Álvarez, L. Calvillo, M.J. Lázaro, E. Pastor, J. Power Sources 195 (2010) 4022–4209.
[23] S.H. Joo, S.J. Choi, I. Oh, J. Kwak, Z. Liu, O. Terasaki, R. Ryoo, Nature 412 (2001) 169–172.
[24] J.W. Lee, S.H. Yoon, T.H. Hyeon, S.M. Oh, K.B. Kim, Chem. Commun. 34 (1999) 2177–2178.
[25] Z. Li, M. Jaroniec, J. Am. Chem. Soc. 123 (2001) 9208–9209.
[26] S.B. Yoon, J.Y. Kim, J.S. Yu, Chem. Commun. 14 (2002) 1536–1537.
[27] C. Liang, Z. Li, S. Dai, Angew. Chem. Int. Ed. 47 (2008) 3696–3717.
[28] J. Lee, J. Kim, T. Hyeon, Adv. Mater. 18 (2006) 2073–2094.
[29] B. Hu, K. Wang, L. Wu, S.H. Yu, M. Antonietti, M.M. Titirici, Adv. Mater. 22 (2010) 813–828.
[30] Y. Wan, Y. Shi, D. Zhao, Chem. Mater. 20 (2008) 932–945.
[31] R. Grieken, J. Iglesias, V. Morales, R.A. García, Micropor. Mesopor. Mater. 131 (2010) 321–330.
[32] A. Palani, H.Y. Wu, C.C. Ting, S. Vetrivel, K. Shanmugapriya, A.S.T. Chiang, M.H. Kao, Micropor. Mesopor. Mater. 131 (2010) 385–392.
[33] O.A. Anunziata, A.R. Beltramone, M.L. Martínez, L.L. Belon, J. Colloid Interface Sci. 315 (2007) 184–190.
[34] S.K. Das, M.K. Bhunia, A. Bhaumik, J. Solid State Chem. 183 (2010) 1326–1333.
[35] M. Armandi, B. Bonelli, C.O. Areán, E. Garrone, Micropor. Mesopor. Mater. 112 (2008) 411–418.
[36] M. Armandi, B. Bonelli, E.I. Karaindrou, C.O. Areán, E. Garrone, Catal. Today 138 (2008) 244–248.
[37] P.C. Eklund, J.M. Holden, R.A. Jishi, Carbon 33 (1995) 959–972.
[38] K. Xia, Q. Gao, C. Wu, S. Song, M. Ruan, Carbon 45 (2007) 1989–1996.

[39] T. Roussel, R.J.M. Pellenq, M. Bienfait, C. Vix-Guterl, R. Gadiou, F. Béguin, M. Johnson, Langmuir 22 (2006) 4614–4619.
[40] L. Vradman, L. Titelman, M. Herskowitz, Micropor. Mesopor. Mater. 93 (2006) 313–317.
[41] C. Vix-Guterl, E. Frackowiak, K. Jurewicz, M. Friebe, J. Parmentier, F. Béguin, Carbon 43 (2005) 1293–1302.
[42] B.Z. Fang, H.S. Zhou, I. Honma, J. Phys. Chem. B 110 (2006) 4875–4880.
[43] B.J. Kim, S.J. Park, J. Colloid Interface Sci. 311 (2007) 619–621.
[44] K. Xia, Q. Gao, S. Song, C. Wu, J. Jiang, J. Hu, L. Gao, Int. J. Hydrogen Energy 33 (2008) 116–123.
[45] S.K.W. Sing, D.H. Everett, R.A.W. Haul, L. Moscou, R.A. Pierotti, J. Rouquerol, Pure Appl. Chem. 57 (1985) 603–619.
[46] H.M. Yoo, S.Y. Lee, B.J. Kim, S.J. Park, Carbon Lett. 12 (2011) 112–115.
[47] J.J. Purewal, H. Kabbour, J.J. Vajo, C.C. Ahn, B. Fultz, Nanotechnology 20 (2009) 204012–204018.
[48] L. Zubizarreta, A. Arenillas, J.J. Pis, Int. J. Hydrogen Energy 34 (2009) 4575–4581.
[49] S.Y. Lee, S.J. Park, Int. J. Hydrogen Energy 35 (2010) 6757–6762.
[50] H. Zhu, X. Li, L. Ci, C. Xu, D. Wu, Z. Mao, Mater. Chem. Phys. 78 (2003) 670–675.